Strain Rate Dissipation for Elastic Deformations

Rosa M. Sánchez-Banderas   Miguel A. Otaduy

Universidad Rey Juan Carlos, Madrid

Figure 1: *With strain rate dissipation potentials, we ensure by construction that damping forces affect only motions that produce a change of deformation. The damping model is simple yet rich and versatile, as demonstrated by the examples. We have tested strain rate dissipation potentials on cloth simulations modeled with StVK elasticity and with yarns with sliding persistent contacts. The snapshots show a yarn-level shirt with over one million nodes.*

Abstract
Damping determines how the energy in dynamic deformations is dissipated. The design of damping requires models where the behavior along deformation modes is easily controlled, while other motions are left unaffected. In this paper, we propose a framework for the design of damping using dissipation potentials formulated as functions of strain rate. We study simple parameterizations of the models, the application to continuum and discrete deformation models, and practical implications for implementation. We also study previous simple damping models, in particular we demonstrate limitations of Rayleigh damping. We analyze in detail the application of strain rate dissipation potentials to two highly different deformation models, StVK hyperelasticity and yarn-level cloth with sliding persistent contacts. These deformation models are representative of the range of applicability of the damping model.

CCS Concepts
•*Computing methodologies* → *Physical simulation;*

1. Introduction

Damping is a defining characteristic of real-world deformable objects. It determines the duration of oscillations, and hence the perception of dynamics and sound. Due to this relevance, it becomes a basic ingredient of physics-based computer animated deformations.

However, despite the omnipresence of damping, its study has received far less attention than its companion elasticity. Few works have been explicitly dedicated to the problem, with notable exceptions to avoid spurious damping [SSF13], estimate model parameters [BTH*03], or design damping behaviors in an artist-friendly manner [XB17]. Perhaps due to the limited attention, many computer animation works have used simplistic damping models, such as Rayleigh damping [Ray96]. In our experience, this approach turns problematic when fine control is necessary, either for artistic design or to match real-world behaviors.

In this work, we study the design of simple damping models that satisfy important conditions by construction. In particular, we seek forces that damp only the change of deformation, and leave other dynamics unaffected. Such conditions have been advocated before [BW98, BMF03], but we formalize the requirements for *good damping* and establish a framework for the design of simple damping models.

We build our damping model on top of the concept of dissipation potential from classical mechanics [GPS14]. This approach parallels the design of elastic deformation models based on energy formulations [XSZB15, MMO16], and same as energy-based elastic models simplify the enforcement of good elasticity conditions, dissipation potentials simplify the enforcement of good damping conditions. As described in Section 3, we propose a framework for damping models with dissipation potentials based on strain rate. This framework also helps us demonstrate why the popular Rayleigh damping model fails for nonlinear deformation models.

Furthermore, we develop diverse applied examples that prompt the considerations to be addressed for practical implementations. In Section 4, we discuss the application of strain rate dissipation potentials to the Saint-Venant Kirchhoff (StVK) hyperelasticity model [SB12]. In this setting, we study the design of continuum dissipation models and their discretization, possibilities for parameterization under multi-dimensional strain metrics, and implications of implicit integration. In Section 5, we discuss the application of strain rate dissipation potentials to yarn-level cloth simulation with sliding persistent contacts [CLMMO14]. This model allows us to analyze the application to discretizations that combine Lagrangian and Eulerian coordinates. In addition, damping of yarn bending gives rise to challenges in the design of strain metrics, which are not present in elastic deformations alone.

We have evaluated the implementation of strain rate dissipation potentials on StVK elasticity for cloth simulation as well as yarn-level cloth (the latter shown in Fig. 1). Thanks to their diversity, these two examples cover many aspects of elastic deformation models, namely, nonlinear, multidimensional, and/or angular deformation metrics, as well as Lagrangian and mixed Lagrangian-Eulerian discretizations.

2. Related Work

The energy stored in oscillating mechanical systems may be dissipated due to several reasons: collisions, friction, or ultimately the resistance of matter to change its current shape or structure. All these dissipative effects are grouped under *damping*. Computer animation has addressed the simulation of materials and effects with very diverse damping behaviors, from the highly damped behavior of flesh to the inviscid behavior of water.

Computer animation works usually distinguish three distinct types of damping, depending on their nature and purpose. (i) Damping that is deliberately formulated in order to simulate the nature of the given material is often referred to as *material-intrinsic damping* [CK05]. (ii) Damping produced by implicit formulations of the system dynamics is referred to as *artificial* or *numerical damping*. (iii) Damping added to enhance stability is usually referred to as *fictitious damping* [YKC00]. In our work, we focus on material-intrinsic damping; therefore, our purpose is to model internal dissipative forces resulting from changes in the object or material state.

The first step in the design of a damping model is to identify the relevant state variables that determine energy dissipation. The most common approach is to assume that dissipation is determined by instantaneous velocities, which gives rise to velocity-dependent potentials, such as Rayleigh's dissipation function [Ray96]. Many works in computer animation implement linear damping models that fit this category [OSG02, GHDS03, BJ05, CLMMO14, GSS*15, XB17]. Linear damping models are well suited for linear deformation models, but as we demonstrate in this paper, they fail for nonlinear deformation models.

Baraff and Witkin [BW98] paid attention to the design of good dissipation models for dynamic deformations. They defined damping forces aligned with soft-constraint elastic forces, but proportional to constraint velocities instead. Oh et al. [OAW06] identified that semi-implicit integration adds artificial damping, and further improved the work of Baraff and Witkin with an implicit integration technique that is able to reproduce stable cloth without introducing excessive damping forces.

Inadvertently, Baraff and Witkin designed a damping model that constitutes a particular case of dissipation potential [GPS14], defined as a quadratic function of constraint velocities. Recently, dissipation potentials were revisited as quadratic functions of strain rate, and applied to yarn-level cloth simulation with mixed Lagrangian-Eulerian discretization [SBO17]. In our work, we formalize the design of dissipation potentials as functions of strain rate, analyze theoretically their benefits and the pitfalls of Rayleigh damping, and discuss parameterization, discretization, and implementation aspects. We also pick yarn-level cloth simulation as one of our target examples, and we revisit and generalize the observations in [SBO17] about the application of dissipation potentials.

We test our damping modeling framework on cloth simulation examples. Terzopoulos et al. [TPBF87] were the first to add damping forces to cloth simulation in computer graphics. They implemented a simple viscous drag force, which damps all types of motion, not only deformations. Carignan et al. [CYTT92] recognized the need for damping functions which do not penalize rigid-body motion of the cloth, hence they added a force which damps cloth stretch and shear. Nevertheless, their damping function is linear in velocities, and suffers the limitations of Rayleigh damping. Volino and Magnenat-Thalmann [VMT00, VMT01] observed that inappropriate damping forces may prevent wrinkles from forming or disappearing correctly, or may prevent fabrics even from falling under their own weight. Choi and Ko [CK05] proposed a method that includes artificial damping and material-intrinsic damping, but avoids fictitious damping through the use of a predicted static post-buckling response as an effective way of handling the instabilities associated with post-buckling situations.

The design of damping forces has also received attention in other contexts in computer animation. Variational integrators aim to preserve dynamic invariants accurately, and one of their results is to minimize numerical damping [KYT*06, GSS*15]. Su et al. [SSF13] designed a simulation method that preserves energy by monitoring undesired energy dissipation, which is restored into the system.

Several authors have proposed methods for the estimation of dissipative models from measurements, such as damping coefficients from video [BTH*03], internal friction parameters from force-deformation measurements [MTB*13], or damping coefficients from sound [PDJ*01]. The recent work of Xu and Barbič [XB17] introduces a method to design damping behaviors in an

artist-friendly manner. Starting from a regular Rayleigh damping model, they modify the damping behavior for arbitrary deformation directions.

Beyond the simulation of dynamic deformation of solid objects, the design of dissipation models has received attention in the context of fluid animation. In that context, most works have focused their efforts on the accurate yet efficient reproduction of complex effects under the dynamic topology of fluids. Some examples include implicit viscosity formulations for the simulation of highly viscous fluid materials and melting effects [CMIT02], or accurate handling of buckling and coiling in free-surface viscous flows [BB08].

3. Dissipation Potentials for Good Damping

In this section, we describe and analyze the damping model based on strain rate dissipation potentials. We start by defining the desired properties of a good damping model. Then, we introduce strain rate dissipation potentials and the generic derivation of damping forces. We follow with practical considerations for the implementation of strain rate dissipation potentials on continuum and discrete elastic deformation models. And we discuss the computation of force Jacobians for implicit integration.

To conclude the section, we compare strain rate dissipation potentials to other simple damping models used in computer animation. In particular, for the Rayleigh damping model, we provide theoretical and experimental analysis.

3.1. Good Damping

Let us assume that deformation is measured through some generic strain metric ε. We define that a certain velocity $\mathbf{v}$ is decoupled from deformation if it produces no strain rate, or change of deformation, i.e., $\dot{\varepsilon} = \nabla_{\mathbf{x}}\varepsilon^T \mathbf{v} = 0$. In other words, a velocity that is decoupled from deformation lies on the null-space of the strain gradient $\nabla_{\mathbf{x}}\varepsilon$.

We define *good damping* as the dissipative forces $\mathbf{f}_d$ that produce no effect on velocities that are decoupled from deformation. Even though real-world dissipative forces may also act on velocities that are decoupled from deformation, such relationship is complex and generally unknown. Then, our strategy is to model coupled and decoupled damping separately, as also advocated by others before [BW98, BMF03]. From the definition of velocities that are decoupled from deformation, good damping implies that dissipative forces have a null projection onto the null-space of the strain gradient, i.e.,

$$\left(\mathbf{I} - \nabla_{\mathbf{x}}\varepsilon \left(\nabla_{\mathbf{x}}\varepsilon^T \nabla_{\mathbf{x}}\varepsilon \right)^{-1} \nabla_{\mathbf{x}}\varepsilon^T \right) \mathbf{f}_d = 0. \quad (1)$$

3.2. Strain Rate Dissipation Potential

We model dissipation using the concept of dissipation potential from classical mechanics [GPS14]. Given a dissipation potential V_d, dissipative forces are obtained as the negative velocity-gradient of the dissipation potential. These forces can be added to the regular Euler-Lagrange equations. For a system with kinetic energy $T = \frac{1}{2}\mathbf{v}^T \mathbf{M}\mathbf{v}$, conservative potential V_e, and dissipation potential

V_d, the Euler-Lagrange equations on reduced coordinates $\mathbf{x}$, with velocities $\mathbf{v} = \dot{\mathbf{x}}$, are:

$$\mathbf{M}\dot{\mathbf{v}} = \nabla_{\mathbf{x}}T - \nabla_{\mathbf{x}}V_e - \nabla_{\mathbf{v}}V_d - \dot{\mathbf{M}}\mathbf{v}. \quad (2)$$

We propose to define the dissipation potential in terms of the strain rate metric $\dot{\varepsilon}$, i.e., $V_d(\dot{\varepsilon})$. Then, the dissipative forces $\mathbf{f}_d$ can be expressed as

$$\mathbf{f}_d = -\nabla_{\mathbf{v}}V_d = -\nabla_{\mathbf{x}}\varepsilon \nabla_{\dot{\varepsilon}}V_d. \quad (3)$$

The term $\nabla_{\dot{\varepsilon}}V_d$ can be regarded as an (integrated) dissipative stress. Then, we observe that strain rate dissipation potentials produce dissipative forces that can be obtained by projecting a dissipative stress onto the space of motions defined by the strain gradient. And it follows that these dissipative forces have a null projection onto the null-space of the strain gradient. We can confirm this by plugging the dissipative forces (3) into (1), and we conclude that strain rate dissipation potentials satisfy the good damping condition by construction.

3.3. Integration of Potential Densities

Furthermore, we consider a particular type of potential, obtained by integrating potential densities. We start from an elastic potential, defined in terms of some multi-dimensional strain metric ε, i.e.,

$$V_e = \sum_i w_i \Psi_{e,i}(\varepsilon), \quad (4)$$

where $\Psi_{e,i}(\varepsilon)$ is a strain energy density evaluated on some integration point, and w_i is the corresponding weight. Such integrated models are ubiquitous, and they encompass both discrete elastic models, as well as FEM models where energies are evaluated using quadrature formulations. Note that, for example, the simple FEM model with linear basis functions on simplicial meshes corresponds to the case where the strain energy density is evaluated once per mesh element, and the integration weight is the volume of the element.

From the elastic potential above, we may derive elastic forces $\mathbf{f}_e$. For Lagrangian discretizations, where integration weights w_i are constant, the elastic forces can be obtained as

$$\mathbf{f}_e = -\nabla_{\mathbf{x}}V_e = -\sum_i w_i \nabla_{\mathbf{x}}\varepsilon \mathbf{S}_{e,i}. \quad (5)$$

Here, the term $\mathbf{S}_{e,i} = \nabla_{\varepsilon}\Psi_{e,i}$ is, by definition, the *elastic stress*.

We define similarly a dissipation potential, by integrating dissipation potential densities that depend on the strain rate $\dot{\varepsilon}$:

$$V_d = \sum_i w_i \Psi_{d,i}(\dot{\varepsilon}). \quad (6)$$

And we derive the corresponding dissipative forces:

$$\mathbf{f}_d = -\nabla_{\mathbf{v}}V_d = -\sum_i w_i \nabla_{\mathbf{x}}\varepsilon \mathbf{S}_{d,i}. \quad (7)$$

Here, $\mathbf{S}_{d,i} = \nabla_{\dot{\varepsilon}}\Psi_{d,i}$ is the *dissipative stress*.

By contrasting (7) and (5), we can conclude that, for purely Lagrangian discretizations, elastic and dissipative forces can be obtained by following a similar procedure. In both cases, they can be obtained as weighted sums of the respective stress values multiplied

by the strain gradient. In Section 5 we visit the case of recently popular mixed Lagrangian-Eulerian discretizations, which do not follow the same pattern.

3.4. Force Jacobians

Implicit integration methods require the computation of force Jacobians for the linearization of accelerations. Damping forces (7) depend on both positions and velocities, hence we need both Jacobians.

The Jacobian w.r.t. velocities is:

$$\frac{\partial \mathbf{f}_d}{\partial \mathbf{v}} = -\sum_i w_i \, \nabla_{\mathbf{x}} \varepsilon \, \frac{\partial \mathbf{S}_{d,i}}{\partial \dot{\varepsilon}} \, \nabla_{\mathbf{x}} \varepsilon^T. \tag{8}$$

This Jacobian is typically not problematic. The term $\frac{\partial \mathbf{S}_{d,i}}{\partial \dot{\varepsilon}}$ is symmetric and, for the case of quadratic dissipation potentials, constant. In that case, positive definiteness can easily be enforced.

The Jacobian w.r.t. positions is:

$$\frac{\partial \mathbf{f}_d}{\partial \mathbf{x}} = -\sum_i w_i \left(\frac{\partial^2 \varepsilon}{\partial \mathbf{x}^2} \, \mathbf{S}_{d,i} + \nabla_{\mathbf{x}} \varepsilon \, \frac{\partial \mathbf{S}_{d,i}}{\partial \dot{\varepsilon}} \, \nabla_{\mathbf{x}} \dot{\varepsilon}^T \right). \tag{9}$$

This Jacobian may be problematic for two reasons. The second term is not symmetric, and we choose to discard it. The first term, on the other hand, may not be positive definite. To enforce positive definiteness, we propose to clamp the negative eigenvalues of the stress $\mathbf{S}_{d,i}$. Note that a similar term $\frac{\partial^2 \varepsilon}{\partial \mathbf{x}^2} \mathbf{S}_{e,i}$ arises in the Jacobian $\frac{\partial \mathbf{f}_e}{\partial \mathbf{x}}$ of elastic forces (5); therefore, implicit integration of damping forces based on strain rate dissipation potentials does not add notable complexity or cost.

We have validated that the two modifications to the Jacobian are beneficial in practice. We have tested them on implicit integration with Newmark and backward Euler methods with full Newton solves, and in the backward Euler case also with just one Newton iteration. The modifications to the Jacobian provide faster convergence of the Newton solves, as they enable the use of fast solvers for symmetric positive-definite matrices. Under just one Newton iteration, we have observed a slight difference in kinetic energy (less than 2% in our tests), which is far less than the error introduced by exiting the solve early.

3.5. Damping Models in Computer Animation

Baraff and Witkin [BW98] designed dissipative forces for soft constraints, where their constraints can be paralleled to strain metrics. Their formulation enforces that dissipative forces are aligned with constraint gradients, hence they satisfy the good damping condition by construction. Our strain rate dissipation potentials can be regarded as a generalization of their dissipative forces. By working with dissipation potentials, and not directly with forces as they do, our formulation supports arbitrary nonlinearity, anisotropy, etc., while theirs is limited to quadratic dissipation potentials. Furthermore, by integrating potential densities as described in Section 3.3, our formulation enables a discretization-independent parameterization.

A very common damping model in computer animation is the

Rayleigh dissipation function [Ray96], which defines a generic dissipation potential that is quadratic on the velocities, i.e., $V_d = \frac{1}{2} \mathbf{v}^T \mathbf{D} \mathbf{v}$. Unfortunately, there is no guarantee that the resulting forces satisfy the good damping condition.

As a particular case of Rayleigh dissipation function, the Rayleigh damping model chooses $\mathbf{D} = \alpha \mathbf{M} + \beta \frac{\partial^2 V_e}{\partial \mathbf{x}^2}$. The scalar values α and β weight, respectively, the mass matrix and the Hessian of the elastic energy (or tangent stiffness matrix). These two terms are supposed to provide damping of absolute motion and change of deformation respectively, hence $\alpha = 0$ is a trivial requirement for our condition of good damping. From (5), and assuming a purely Lagrangian discretization, we conclude that the tangent stiffness matrix can be expressed in terms of the strain gradient as

$$\frac{\partial^2 V_e}{\partial \mathbf{x}^2} = \frac{\partial^2 \varepsilon}{\partial \mathbf{x}^2} \nabla_\varepsilon V_e + \nabla_{\mathbf{x}} \varepsilon \, \frac{\partial^2 V_e}{\partial \varepsilon^2} \, \nabla_{\mathbf{x}} \varepsilon^T. \tag{10}$$

With $\alpha = 0$, the resulting Rayleigh damping force is

$$\mathbf{f}_R = -\beta \left(\frac{\partial^2 \varepsilon}{\partial \mathbf{x}^2} \nabla_\varepsilon V_e + \nabla_{\mathbf{x}} \varepsilon \, \frac{\partial^2 V_e}{\partial \varepsilon^2} \, \nabla_{\mathbf{x}} \varepsilon^T \right) \mathbf{v}. \tag{11}$$

By plugging this force in the good damping condition (1), we conclude that Rayleigh damping is *good* damping only if the strain metric is linear, i.e., $\frac{\partial^2 \varepsilon}{\partial \mathbf{x}^2} = 0$. Unfortunately, linear strain metrics fail for large deformations. In the next section, we analyze the effect of Rayleigh damping on a simple experiment. Another corollary is that, by dropping the offending term of the stiffness matrix, we can obtain good Rayleigh damping which is equivalent to the following strain rate dissipation potential:

$$V_d = \frac{1}{2} \beta \dot{\varepsilon}^T \frac{\partial^2 V_e}{\partial \varepsilon^2} \dot{\varepsilon}. \tag{12}$$

3.6. Experimental Analysis: Damping a Linear Spring

Let us consider a linear spring on a horizontal plane, with one moving end-point $\mathbf{x}$ and the other end-point fixed at the origin, as shown in Fig. 2. With rest-length L, the strain of the spring is $\varepsilon = \frac{\|\mathbf{x}\|}{L} - 1$. It follows that the strain gradient is $\nabla_{\mathbf{x}} \varepsilon = \frac{1}{L} \cdot \frac{\mathbf{x}}{\|\mathbf{x}\|}$, the strain Hessian is $\frac{\partial^2 \varepsilon}{\partial \mathbf{x}^2} = \frac{1}{L} \left(\mathbf{I} - \frac{\mathbf{x}}{\|\mathbf{x}\|} \frac{\mathbf{x}^T}{\|\mathbf{x}\|} \right)$, and the strain rate is $\dot{\varepsilon} = \frac{1}{L} \cdot \frac{\mathbf{x}^T}{\|\mathbf{x}\|} \dot{\mathbf{x}}$. We design a quadratic elastic energy of the form $V_e = \frac{1}{2} L k_e \varepsilon^2$, Rayleigh damping with $\alpha = 0$, and an *equivalent* strain rate dissipation potential given by (12).

In Fig. 2 we plot kinetic energy profiles for several animations where we compare Rayleigh damping and strain rate dissipation potentials. In all the animations, the moving end-point is initialized with a velocity of 20 tangent to the spring, with the spring undeformed. The simulation parameters were: rest-length $L = 2$, elastic stiffness $k_e = 100$, mass $m = 1$. Fig. 2 compares the behavior for several values of β. With strain rate dissipation potentials, damping affects only the oscillation of the spring length, and the system reaches a uniform circular motion where the elastic force acts as centripetal force. With Rayleigh damping, the system slows down toward a full stop.

The results were obtained with a time step of 0.01, and are practically identical for symplectic Euler and implicit Newmark, hence
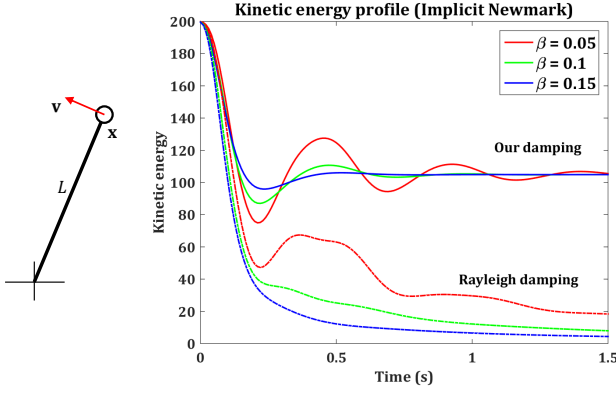
Figure 2: *We simulate a spring rotating on a horizontal plane under different damping models. Left: Initial conditions, with mass at position $\mathbf{x}$ and velocity $\mathbf{v}$ tangent to the spring, of rest-length L. Right: Evolution of the kinetic energy with our strain rate dissipation potential Vs. Rayleigh damping, for three different values of damping coefficient β. The dissipation potential is modeled according to (12) in this experiment.*

we can rule out effects due to the integration method. Backward Euler, on the other hand, suffers noticeable numerical damping, however far less than the one introduced by Rayleigh damping. With implicit Newmark and a time step of 0.1, the damping behavior is still well preserved under a full Newton solve, while exiting the Newton solve after one iteration introduces some error, again far less than the error introduced by Rayleigh damping.

4. Example 1: StVK Elasticity

We choose the StVK elastic material model as an example of hyperelasticity. In this section, we study the application of strain rate dissipation potentials to this deformation model, and we propose a parameterization that produces a linear isotropic dissipative stress.

Given deformed and undeformed positions $\mathbf{x}$ and $\bar{\mathbf{x}}$ respectively, the deformation gradient is defined as $\mathbf{F} = \frac{\partial \mathbf{x}}{\partial \bar{\mathbf{x}}}$. Then, the Green strain tensor is defined as $\varepsilon = \frac{1}{2}\left(\mathbf{F}^T \mathbf{F} - \mathbf{I}\right)$, and the StVK elastic material model defines a strain energy density

$$\Psi_e = \frac{\lambda}{2}\operatorname{tr}(\varepsilon)^2 + \mu\operatorname{tr}\left(\varepsilon^2\right), \tag{13}$$

with λ and μ the Lamé constants.

This energy definition yields the second Piola-Kirchhoff stress

$$\mathbf{S}_e = \nabla_\varepsilon \Psi_e = \lambda \operatorname{tr}(\varepsilon)\,\mathbf{I} + 2\mu\varepsilon. \tag{14}$$

The use of a nonlinear strain metric turns the complete model non-linear, yet the stress-strain relationship is linear and isotropic.

Based on the integral formulation (4) of the StVK strain energy density (13), we could define a dissipation potential for StVK by following the Rayleigh damping analogy (12). However, strain rate dissipation potentials allow much more versatile formulations.

Here, we explore one example, using a parameterization anologous to the StVK strain energy density (13). We formulate an analogous dissipation potential, substituting the strain with the strain rate:

$$\Psi_d = \frac{\lambda_d}{2}\operatorname{tr}(\dot{\varepsilon})^2 + \mu_d\operatorname{tr}\left(\dot{\varepsilon}^2\right), \tag{15}$$

We consider two independent material parameters λ_d and μ_d, analogous to the Lamé parameters for the elastic case. Interestingly, isotropic Newtonian fluids are also parameterized by two parameters, typically the dynamic viscosity and the bulk viscosity. However, the mapping to these two parameters is unclear, as they are defined for a different strain rate tensor.

Our proposed dissipation potential definition yields the following linear isotropic dissipative stress:

$$\mathbf{S}_d = \nabla_{\dot{\varepsilon}}\Psi_d = \lambda_d\operatorname{tr}(\dot{\varepsilon})\,\mathbf{I} + 2\mu_d\dot{\varepsilon}. \tag{16}$$

This formulation enables very simple implementation in practice, as discussed in Section 3.3. At each integration point, the dissipative stress is evaluated and added to the second Piola-Kirchhoff stress, and the rest of the force computation follows as usual. The evaluation of the dissipative stress requires the strain rate, which is obtained by differentiating the Green strain tensor, and yields:

$$\dot{\varepsilon} = \frac{1}{2}\left(\mathbf{F}^T\dot{\mathbf{F}} + \dot{\mathbf{F}}^T\mathbf{F}\right). \tag{17}$$

The time derivative of the deformation gradient is nothing else but the gradient of the velocity w.r.t. undeformed coordinates, i.e., $\dot{\mathbf{F}} = \frac{\partial \mathbf{v}}{\partial \bar{\mathbf{x}}}$. For linear shape functions, the deformation gradient is obtained per element as $\mathbf{F} = \mathbf{X}\cdot\bar{\mathbf{X}}^{-1}$, where $\mathbf{X}$ is a matrix built with element node positions as columns, and $\bar{\mathbf{X}}$ is a constant matrix that depends on undeformed node positions [SB12]. The time derivative of the deformation gradient can be obtained similarly as $\dot{\mathbf{F}} = \mathbf{V}\cdot\bar{\mathbf{X}}^{-1}$, where $\mathbf{V}$ is a matrix built with element node velocities as columns.

The dissipative stress (16) could be applied also to other deformation models. One example is corotational elasticity, with strain $\varepsilon = \mathbf{R}^{-1}\mathbf{F} - \mathbf{I}$, and $\mathbf{R}$ a rotation matrix obtained through polar decomposition of the deformation gradient $\mathbf{F}$. The implementation would differ in the computation of the gradient and the time derivative of the strain, and we leave the test of such extensions for future work.

As discussed in Section 3.4, the application of the model with implicit integration requires the computation of force Jacobians. With our stress definition (16), ensuring well-behaved Jacobians is simple. In the Jacobian w.r.t. velocities (8), the term $\frac{\partial \mathbf{S}_{d,i}}{\partial \dot{\varepsilon}}$ is constant, symmetric, and also positive definite for the right values of λ_d and μ_d. In the Jacobian w.r.t. positions (9), we do as proposed in Section 3.4, and clamp the negative eigenvalues of the stress $\mathbf{S}_{d,i}$ for each mesh element.

5. Example 2: Yarns with Sliding Persistent Contacts

Cirio et al. [CLMMO14, CLMO17] designed a yarn-level cloth model that represents yarns as flexible rods in persistent contact, but with the option to slide with respect to each other. Their

reduced-coordinate representation combines Lagrangian coordinates for the 3D position of yarn crossings, with Eulerian coordinates for the sliding arc-length positions of such yarn crossings. Thanks to the sliding arc-length coordinates, their method avoids altogether the computation of collision detection and collision response between yarns that are permanently in contact, and handles such inter-yarn contact implicitly.

The model of yarns with sliding persistent contacts poses two interesting questions for the design of good damping. First, due to the existence of Eulerian coordinates, the analysis of elastic and damping forces in Section 3.3 does not hold. Second, the straightforward design of strain rate dissipation potentials for rod bending suffers robustness problems due to indeterminacy of the strain gradient. In this section, we address these two questions, demonstrating the application of strain rate dissipation to yarn-level cloth simulation.

5.1. Forces and their Jacobians

Yarns with sliding persistent contacts constitute a case of mixed Lagrangian-Eulerian discretization [SJLP11, FLLP13]. In such models, the integration weights of elastic energies formulated as (4) are not constant, as they depend on the Eulerian coordinates. Revisiting the derivation of elastic forces, we obtain the following expression:

$$\mathbf{f}_e = -\nabla_{\mathbf{x}} V_e = -\sum_i w_i \nabla_{\mathbf{x}} \varepsilon \nabla_{\varepsilon} \Psi_{e,i} - \sum_i \nabla_{\mathbf{x}} w_i \Psi_{e,i}. \quad (18)$$

Unlike the elastic force (5) for purely Lagrangian discretizations, in this case the elastic force does not point in the direction of the strain gradient $\nabla_{\mathbf{x}} \varepsilon$. It exhibits a term that minimizes elastic energy simply by smearing it out by changing the Eulerian discretization. This term points in the direction $\nabla_{\mathbf{x}} w_i$.

The damping force (7) for Lagrangian discretizations is valid for the mixed Lagrangian-Eulerian case, as the integration weights depend on positions, not velocities. Several authors in the past, notably Baraff and Witkin [BW98], have argued for damping forces that are aligned with elastic forces. As shown here, this should not be the case for mixed Lagrangian-Eulerian discretizations.

In the computation of force Jacobians, the Jacobian w.r.t. positions (9) also needs to be revisited. For mixed Lagrangian-Eulerian discretizations, it turns:

$$\frac{\partial \mathbf{f}_d}{\partial \mathbf{x}} = -\sum_i w_i \left(\frac{\partial^2 \varepsilon}{\partial \mathbf{x}^2} \mathbf{S}_{d,i} + \nabla_{\mathbf{x}} \varepsilon \frac{\partial \mathbf{S}_{d,i}}{\partial \dot{\varepsilon}} \nabla_{\mathbf{x}} \dot{\varepsilon}^T \right) + \nabla_{\mathbf{x}} \varepsilon \mathbf{S}_{d,i} \nabla_{\mathbf{x}} w_i^T. \quad (19)$$

The added term, due to the gradient of the integration weight $\nabla_{\mathbf{x}} w_i$, is not symmetric. Following the same recommendations discussed in Section 3.4, we choose to discard this term.

5.2. Damping for Rod Bending

Cirio et al. [CLMMO14] model individual yarns as twist-free isotropic elastic rods. They are discretized into linear segments, with stretch and bending elastic energies that capture their internal resistance to deformation. Unfortunately, the bending deformation model is problematic for the formulation of strain rate dissipation potentials, due to indeterminacies at small angles. This problematic

behavior is independent of the Eulerian discretization; therefore, we limit our discussion to a purely Lagrangian discretization.
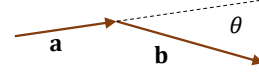
Given two consecutive rod segments as shown above, with segment vectors $\mathbf{a}$ and $\mathbf{b}$, and added rest-length L, bending strain ε_θ can be defined as

$$\varepsilon_\theta = \frac{\theta}{L}, \quad \text{with } \tan\theta = \frac{|\mathbf{a} \times \mathbf{b}|}{\mathbf{a}^T \mathbf{b}}. \quad (20)$$

Others have proposed similar bending strain formulations, using, e.g., $\tan\frac{\theta}{2}$ [BWR*08] or $\sin\frac{\theta}{2}$ [BMF03] instead of the angle θ. However, they are not well behaved for the large bending angles suffered by cloth yarns. $\tan\frac{\theta}{2} \to \infty$ for $\theta \to \pi$, and $\sin\frac{\theta}{2}$ yields a nonconvex energy for $\theta > \frac{\pi}{2}$.

From the strain expression (20), bending strain rate can be derived as $\dot{\varepsilon}_\theta = \frac{\dot{\theta}}{L}$, with angular velocity

$$\dot{\theta} = \frac{\cos^2\theta}{\mathbf{a}^T \mathbf{b}} \left(\left(\mathbf{a}^T \dot{\mathbf{b}} + \mathbf{b}^T \dot{\mathbf{a}} \right) \tan\theta + \frac{(\mathbf{a} \times \mathbf{b})^T}{|\mathbf{a} \times \mathbf{b}|} \left(\mathbf{a} \times \dot{\mathbf{b}} - \mathbf{b} \times \dot{\mathbf{a}} \right) \right). \quad (21)$$

The strain gradient is not defined when the bending angle is $\theta = 0$. This is not a problem for elastic forces (5) as long as the stress cancels out, which is the case, for example, for typical quadratic energies. However, in damping forces (7), the stress at $\theta = 0$ may be arbitrary, leading to an undefined force direction.

The indeterminacy problem at vanishing angles can be circumvented thanks to a small-angle approximation of the bending strain. In particular, and based on the small-angle approximation of the tangent, i.e., $\lim_{\theta \to 0} \frac{\tan\theta}{\theta} = 1$, we propose the following vector strain metric for small bending angles:

$$\varepsilon_{\mathbf{k}} = \frac{\mathbf{k}}{L}, \quad \text{with } \mathbf{k} = \frac{\mathbf{a} \times \mathbf{b}}{\mathbf{a}^T \mathbf{b}}. \quad (22)$$

For quadratic energies, the energy for the large-angle bending strain (20) and the small-angle bending strain (22) are equivalent under small angles, as demonstrated through

$$\lim_{\theta \to 0} \frac{\varepsilon_\theta^2}{\varepsilon_{\mathbf{k}}^T \varepsilon_{\mathbf{k}}} = \lim_{\theta \to 0} \frac{\theta^2}{\|\mathbf{k}\|} = \lim_{\theta \to 0} \frac{\theta^2}{\tan^2\theta} = 1. \quad (23)$$

From the small-angle strain expression (22), bending strain rate can be derived as

$$\dot{\varepsilon}_{\mathbf{k}} = \frac{1}{L} \cdot \frac{1}{\mathbf{a}^T \mathbf{b}} \left(\left(\mathbf{a}^T \dot{\mathbf{b}} + \mathbf{b}^T \dot{\mathbf{a}} \right) \mathbf{k} + \mathbf{a} \times \dot{\mathbf{b}} - \mathbf{b} \times \dot{\mathbf{a}} \right). \quad (24)$$

The small-angle bending strain (22) has a well-defined gradient for vanishing angles; therefore, it enables robust computation of damping forces. For angles larger than a threshold, we switch back to the regular bending strain (20), as the small-angle bending strain tends to infinity for large angles.

6. Results

We have tested the practical implementation of strain rate dissipation potentials on the two deformation models described in Section 4 and Section 5, both applied to cloth simulation. Please see
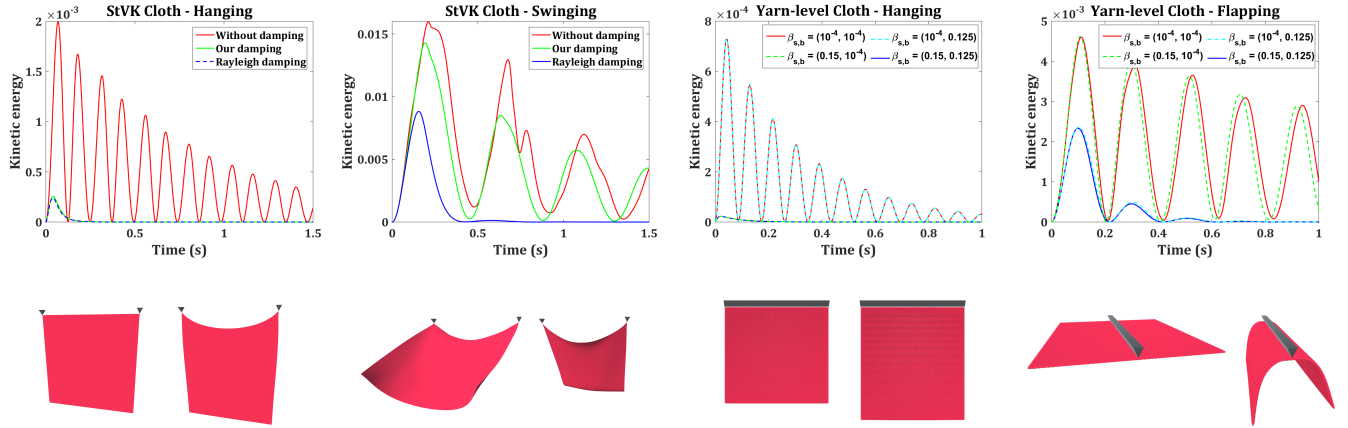
Figure 3: *The plots demonstrate the ability of strain rate dissipation potentials to correctly damp target deformations, leaving others unaffected. All plots show the evolution of kinetic energy under various settings, for the motions depicted beneath. The two plots on the left correspond to the StVK cloth model with no damping, Rayleigh damping with β = 0.15, and our damping tuned to match Rayleigh damping as in (12). Damping is applied only to the membrane StVK model, not to bending. In the 'hanging' motion, our damping and Rayleigh damping produce almost equivalent overdamped motion. In the 'swinging' motion, on the other hand, our model produces a result close to the no-damping case, while Rayleigh suffers high damping. The two plots on the right correspond to the yarn-level cloth model using our damping model, comparing two combinations of stretch damping β_s and two combinations of bending damping β_b. As desired, the stretch damping coefficient determines the behavior in the 'hanging' motion, while the bending damping coefficient determines the behavior in the 'flapping' motion.*

the accompanying video to watch the damping behavior in action. For StVK cloth, we have used the implementation with remeshing available in ARCSim [NSO12]. The simulator uses backward Euler integration with one Newton iteration per time step, and this integration method introduces numerical damping. For yarn-level cloth, we have used the woven cloth simulation method with sliding persistent contacts [CLMMO14], with repulsive forces for collision handling. We use backward Euler numerical integration with adaptive time stepping, with a full Newton solve per time step. Again, the integration method introduces numerical damping. The code is implemented fully on the GPU. The StVK and yarn-level cloth models are not supposed to be compared to each other, as the examples use models of very different resolution, and the parameters do not necessarily produce best-match behaviors.

In Fig. 3 we demonstrate the ability of strain rate dissipation potentials to control damping behavior on specific deformation modes, while leaving other motions unaffected. We have executed two different experiments.

Using the StVK cloth model on a square patch with 1,089 vertices (with remeshing disabled), we compare the behavior with no damping, Rayleigh damping with β = 0.15, and our damping tuned to match Rayleigh damping as in (12). Damping is applied only to membrane deformation, not to bending. The two left plots in Fig. 3 show the evolution of kinetic energy for two different motions ('hanging' and 'swinging'), shown beneath. In the 'hanging' motion, our damping and Rayleigh damping produce almost equivalent overdamped motion. In the 'swinging' motion, on the other hand, our model produces a result close to the no-damping case, while Rayleigh suffers high damping.

Using the yarn-level cloth model on a square patch with 20,402 nodes, we compare the behavior for different values of stretch damping (β_s) and bending damping (β_b). In both cases, we parameterize the dissipation potential following the analogy to Rayleigh damping (12). The two right plots in Fig. 3 show the evolution of kinetic energy for two different motions ('hanging' and 'flapping'), shown beneath. As desired, the stretch damping coefficient determines the behavior in the 'hanging' motion, while the bending damping coefficient determines the behavior in the 'flapping' motion.

We have also tested the strain rate dissipation potentials on larger animations. We have dressed a character model with a shirt, and we have simulated the motion of the shirt using both the StVK and yarn-level cloth models, with two different sets of damping parameters each (medium damping and low damping). The character is animated using publicly available data [PMRMB15]. Fig. 4 shows several snapshots of the animation for each cloth model and choice of damping parameters. Please watch the accompanying video to appreciate the differences in action. In the snapshots, the examples with less damping exhibit more folds.

For the StVK simulation, we have followed the parameterization of dissipation potentials in (15), with the following parameter values: in the medium damping case, $\lambda_d = 30$ and $\mu_d = 20$; in the low damping case, $\lambda_d = 1.5$ and $\mu_d = 1$. With remeshing, the number of vertices in the simulation ranges from 3,300 to 5,976 in the medium damping case, and from 3,386 to 6,926 in the low damping case. Performance varies as the mesh resolution changes, which in turn depends on the amount of dynamics and fine wrinkles. To calibrate performance, we have used a fixed mesh with 10,437 vertices. With a time step of 1.6 ms, the simulation took
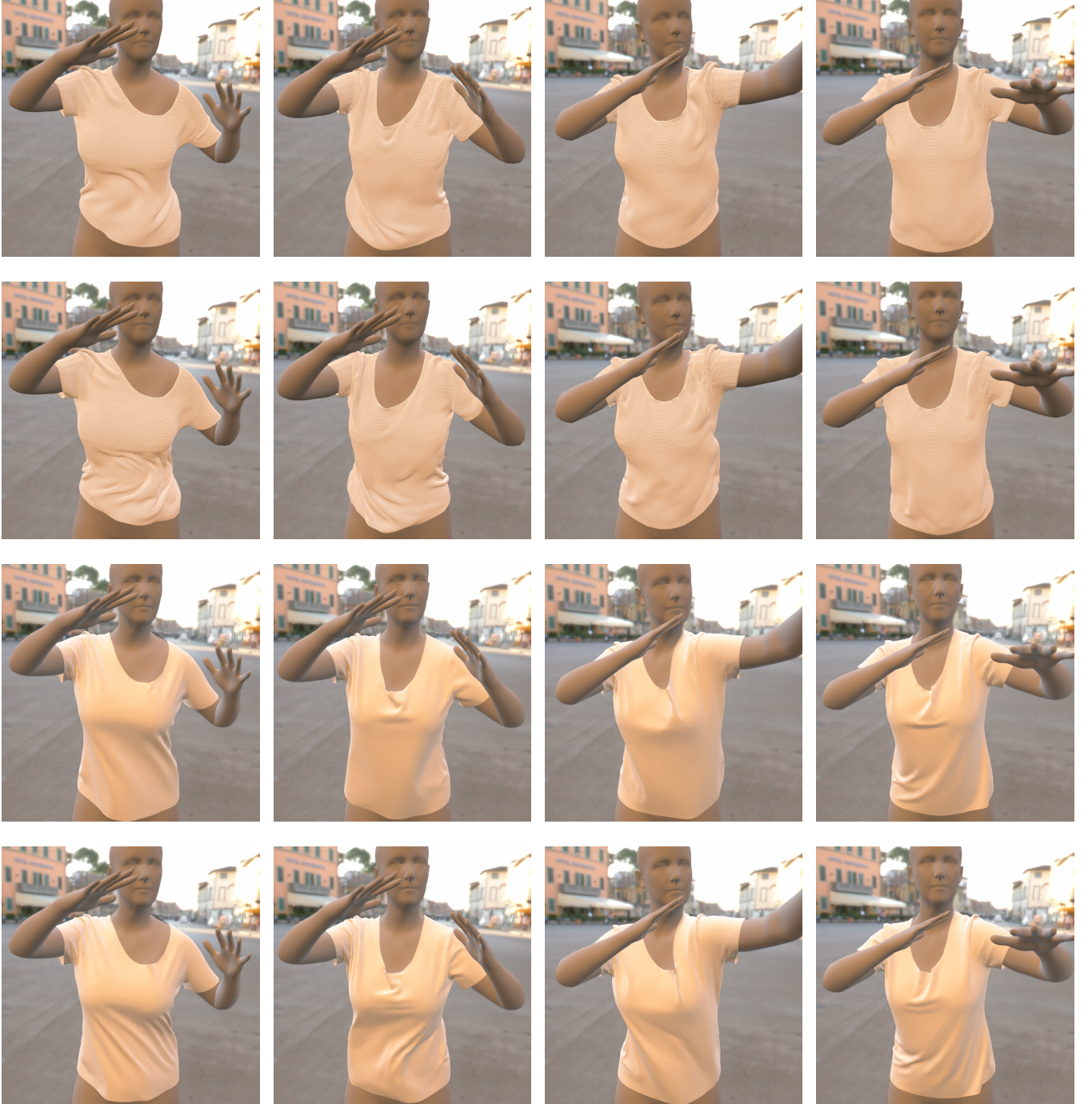
Figure 4: *We compare a simulation of a shirt with two different deformation models and different settings of the strain rate dissipation potentials. From top to bottom: (i) Yarn-level cloth simulation with medium damping ($\beta_s = 0.03$ and $\beta_b = 0.16$); (ii) Yarn-level cloth simulation with low damping ($\beta_s = 3 \times 10^{-4}$ and $\beta_b = 0.016$); (iii) StVK cloth simulation with medium damping ($\lambda_d = 30$ and $\mu_d = 20$); (iv) StVK cloth simulation with low damping ($\lambda_d = 1.5$ and $\mu_d = 1$).*

roughly 1.45 seconds per time step. We have also compared performance w.r.t. the Rayleigh damping model, and dissipation potentials add an overhead of just 2%, due to a slight increase in the cost of collision processing under more vivid dynamics, not due to force computation or solver convergence.

For the yarn-level simulation, we have followed the parameter-

ization of dissipation potentials with the Rayleigh damping analogy described in (12), with the following parameter values: in the medium damping case, stretch damping with $\beta_s = 0.03$ and bending damping with $\beta_b = 0.16$; in the low damping case, stretch damping with $\beta_s = 3 \times 10^{-4}$ and bending damping with $\beta_b = 0.016$. With a shirt with $136,741$ nodes, shown in Fig. 4, and an average time step of 1 ms, the simulation took roughly 9.85 seconds per time step. We have also simulated a higher resolution shirt, shown in Fig. 1, with $1,053,175$ nodes and intermediate damping values of $\beta_s = 3 \times 10^{-3}$ and $\beta_b = 0.1$. With an average time step of 1 ms, the simulation took roughly 86 seconds per time step.

7. Discussion and Future Work

We have presented a framework for the design of damping models, building on the concept of dissipation potentials. We show that a formulation based on strain rate achieves controllable damping for deformation modes, leaving other motions unaffected. We discuss parameterization and implementation aspects, and demonstrate the method on diverse deformation models.

Our approach also suffers some limitations. Since the strain rate is tightly coupled to the choice of strain, the damping model may inherit some limitations of the elastic deformation model. In addition, constraining damping forces to the direction of the strain gradient is the major strength of the model, but it also constitutes a limitation. Our model is not capable of modeling dissipative effects in the null-space of the strain gradient at all, hence it needs to be complemented with other damping forces to achieve such effects. Note, however, that the constitutive model that maps strain rate to dissipation potential may be arbitrarily nonlinear, anisotropic, or heterogeneous, not limited to the characteristics of the elastic constitutive model.

Our work opens interesting avenues for future work. Same as energy-based elastic models set a solid framework for the design of elastic behavior, damping models based on strain rate dissipation potentials set a solid framework for the design of dissipative behavior. The model could be used as an integral building block of measurement-based damping estimation or artist-driven damping design. To this end, it is important to identify artist-friendly parameterizations.

Acknowledgements

References

[BB08] BATTY C., BRIDSON R.: Accurate viscous free surfaces for buckling, coiling, and rotating liquids. In *ACM SIGGRAPH/Eurographics Symp. on Computer Animation* (2008), pp. 219–228. 3

[BJ05] BARBIČ J., JAMES D. L.: Real-time subspace integration for st. venant-kirchhoff deformable models. *ACM Trans. Graph. 24*, 3 (July 2005), 982–990. 2

[BMF03] BRIDSON R., MARINO S., FEDKIW R.: Simulation of clothing with folds and wrinkles. In *Proceedings of the 2003 ACM SIGGRAPH/Eurographics Symposium on Computer Animation* (2003), pp. 28–36. 1, 3, 6

[BTH*03] BHAT K. S., TWIGG C. D., HODGINS J. K., KHOSLA P. K., POPOVIĆ Z., SEITZ S. M.: Estimating cloth simulation parameters from video. In *Proceedings of the 2003 ACM SIGGRAPH/Eurographics Symposium on Computer Animation* (2003), pp. 37–51. 1, 2

[BW98] BARAFF D., WITKIN A.: Large steps in cloth simulation. In *Proceedings of the 25th annual conference on Computer graphics and interactive techniques* (1998), ACM, pp. 43–54. 1, 2, 3, 4, 6

[BWR*08] BERGOU M., WARDETZKY M., ROBINSON S., AUDOLY B., GRINSPUN E.: Discrete elastic rods. *ACM Trans. Graph. 27*, 3 (2008), 63:1–63:12. 6

[CK05] CHOI K.-J., KO H.-S.: Stable but responsive cloth. In *ACM SIGGRAPH 2005 Courses* (2005), ACM, p. 1. 2

[CLMMO14] CIRIO G., LOPEZ-MORENO J., MIRAUT D., OTADUY M. A.: Yarn-level simulation of woven cloth. *ACM Trans. Graph. 33*, 6 (2014), 207:1–207:11. 2, 5, 6, 7

[CLMO17] CIRIO G., LOPEZ-MORENO J., OTADUY M. A.: Yarn-level cloth simulation with sliding persistent contacts. *IEEE Transactions on Visualization and Computer Graphics 23*, 2 (2017), 1152–1162. 5

[CMIT02] CARLSON M., MUCHA P. J., III R. B. V. H., TURK G.: Melting and flowing. In *SIGGRAPH'02* (July 21-22 2002). 3

[CYTT92] CARIGNAN M., YANG Y., THALMANN N. M., THALMANN D.: Dressing animated synthetic actors with complex deformable clothes. In *ACM Siggraph Computer Graphics* (1992), vol. 26, ACM, pp. 99–104. 2

[FLLP13] FAN Y., LITVEN J., LEVIN D. I. W., PAI D. K.: Eulerian-on-lagrangian simulation. *ACM Trans. Graph. 32*, 3 (2013), 22:1–22:9. 6

[GHDS03] GRINSPUN E., HIRANI A. N., DESBRUN M., SCHRÖDER P.: Discrete shells. In *Proceedings of the 2003 ACM SIGGRAPH/Eurographics symposium on Computer animation* (2003), Eurographics Association, pp. 62–67. 2

[GPS14] GOLDSTEIN H., POOLE C. P., SAFKO J. L.: *Classical Mechanics: Pearson New International Edition*. Pearson Higher Ed, 2014. 2, 3

[GSS*15] GAST T. F., SCHROEDER C., STOMAKHIN A., JIANG C., TERAN J. M.: Optimization integrator for large time steps. *IEEE Transactions on Visualization and Computer Graphics 21*, 10 (2015), 1103–1115. 2

[KYT*06] KHAREVYCH L., YANG W., TONG Y., KANSO E., MARSDEN J. E., SCHRÖDER P., DESBRUN M.: Geometric, variational integrators for computer animation. In *Proceedings of the 2006 ACM SIGGRAPH/Eurographics Symposium on Computer Animation* (2006), pp. 43–51. 2

[MMO16] MIGUEL E., MIRAUT D., OTADUY M. A.: Modeling and Estimation of Energy-Based Hyperelastic Objects. *Computer Graphics Forum 35*, 2 (2016), 385–396. 2

[MTB*13] MIGUEL E., TAMSTORF R., BRADLEY D., SCHVARTZMAN S. C., THOMASZEWSKI B., BICKEL B., MATUSIK W., MARSCHNER S., OTADUY M. A.: Modeling and estimation of internal friction in cloth. *ACM Trans. Graph. 32*, 6 (2013), 212:1–212:10. 2

[NSO12] NARAIN R., SAMII A., O'BRIEN J. F.: Adaptive anisotropic remeshing for cloth simulation. *ACM Trans. Graph. 31*, 6 (2012), 152:1–152:10. 7

[OAW06] OH S., AHN J., WOHN K.: Low damped cloth simulation. *The Visual Computer 22*, 2 (2006), 70–79. 2

[OSG02] O'BRIEN J. F., SHEN C., GATCHALIAN C. M.: Synthesizing sounds from rigid-body simulations. In *Proceedings of the 2002 ACM SIGGRAPH/Eurographics Symposium on Computer Animation* (2002), pp. 175–181. 2

[PDJ*01] PAI D. K., DOEL K. V. D., JAMES D. L., LANG J., LLOYD J. E., RICHMOND J. L., YAU S. H.: Scanning physical interaction behavior of 3d objects. In *Proceedings of the 28th Annual Conference on Computer Graphics and Interactive Techniques* (2001), pp. 87–96. 2

[PMRMB15] PONS-MOLL G., ROMERO J., MAHMOOD N., BLACK M. J.: Dyna: A model of dynamic human shape in motion. *ACM Trans. Graph. 34*, 4 (2015), 120:1–120:14. 7

[Ray96] RAYLEIGH J. W. S. B.: *The theory of sound*, vol. 2. Macmillan, 1896. 1, 2, 4

[SB12] SIFAKIS E., BARBIC J.: Fem simulation of 3d deformable solids: A practitioner's guide to theory, discretization and model reduction. In *ACM SIGGRAPH 2012 Courses* (2012), pp. 20:1–20:50. 2, 5

[SBO17] SÁNCHEZ-BANDERAS R. M., OTADUY M. A.: Dissipation Potentials for Yarn-Level Cloth. In *Spanish Computer Graphics Conference (CEIG)* (2017). 2

[SJLP11] SUEDA S., JONES G. L., LEVIN D. I. W., PAI D. K.: Large-scale dynamic simulation of highly constrained strands. *ACM Trans. Graph. 30*, 4 (2011), 39:1–39:10. 6

[SSF13] SU J., SHETH R., FEDKIW R.: Energy conservation for the simulation of deformable bodies. *IEEE Transactions on Visualization and Computer Graphics 19*, 2 (2013), 189–200. 1, 2

[TPBF87] TERZOPOULOS D., PLATT J., BARR A., FLEISCHER K.: Elastically deformable models. In *ACM Siggraph Computer Graphics* (1987), vol. 21, ACM, pp. 205–214. 2

[VMT00] VOLINO P., MAGNENAT-THALMANN N.: Implementing fast cloth simulation with collision response. In *Computer Graphics International* (2000), vol. 2000, pp. 257–266. 2

[VMT01] VOLINO P., MAGNENAT-THALMANN N.: Comparing efficiency of integration methods for cloth simulation. In *Computer graphics international 2001. Proceedings* (2001), IEEE, pp. 265–272. 2

[XB17] XU H., BARBIČ J.: Example-based damping design. *ACM Trans. Graph. 36*, 4 (2017), 53:1–53:14. 1, 2

[XSZB15] XU H., SIN F., ZHU Y., BARBIČ J.: Nonlinear material design using principal stretches. *ACM Trans. Graph. 34*, 4 (2015), 75:1–75:11. 2

[YKC00] YU W., KANG T., CHUNG K.: Drape simulation of woven fabrics by using explicit dynamic analysis. *Journal of the Textile Institute 91*, 2 (2000), 285–301. 2